Chemical Engineering Journal 531 (2026) 173667

Contents lists available at ScienceDirect

Chemical Engineering Journal

journal homepage: www.elsevier.com/locate/cej

Recycling of Li-ion batteries: hydrometallurgical flowchart, multivariate analysis, and life cycle assessment

Lucas Fonseca Guimaraes [a,b], Carine de Menezes Rebello [c], Idelfonso Bessa dos Reis Nogueira [c], Mentore Vaccari [b], Denise Crocce Romano Espinosa [a], Amilton Barbosa Botelho Junior [c,*]

[a] Department of Chemical Engineering, Polytechnical School, University of São Paulo, São Paulo, SP, Brazil
[b] Dipartimento di Ingegneria Civile, Architettura, Territorio e Ambiente e di Matematica (DICATAM), Università degli Studi di Brescia, Italy
[c] Department of Chemical Engineering, Norwegian University of Science and Technology, Trondheim, Norway

ARTICLE INFO

Keywords:
Critical minerals
Ni-rich batteries
LCA
Process modeling

ABSTRACT

In this paper, we are proposing a flexible flowchart for recycling Ni-rich Li-ion batteries by hydrometallurgy. Physical separation processing is important to separate cathode and anode fractions from plastic, external structure and foils (mostly Cu). Al foil partly remained in the black mass works as reducing agent reducing costs and environmental impacts of H_2O_2 use. H_2SO_4 is still the best option considering economic and environmental benefits. Mn separation occurs by ozone precipitation demonstrating a better option than solvent extraction reaching 99% efficiency with 96% purity. Ni and Co separation by ion exchange chelating resins (bis-picolylamine) has higher selectivity over Al and Li, and our experimental data and optimization modeling demonstrates that minor differences in particle size of resin beads impacts on adsorption capacity (Dowex M4195 < Lewatit TP 220). About 1.46×10^6 kg-CO_2eq would be generated to produce 1 ton of LiOH, lower than mining process with recovery of 95% battery materials. The process could be used for recycling NMCs, NCA, and LCO cathode-type batteries with minor changes in process steps.

1. Introduction

Popularization of electric vehicles and consequently Li-ion batteries occur as alternative to reducing CO_2 emissions in transportation [1–3]. As a consequence of growing demand for Li-ion batteries [4–6], the search of raw materials is critical to support the demand [1,7]. Although mining will continue to be important, future scenarios run up against production and environmental impact [8–10]. First, production of critical minerals is geographically limited (e.g. >70% of Li production occurs in Chile, Argentina, Australia, China and Brazil) [11,12]; second, several environmental impacts occur in non-sustainable mining exploration [13]. As alternative, recycling of spent Li-ion batteries is interesting due to i) lower environmental impact [14]; ii) higher concentration of critical metals in comparison to natural resources [15,16]; iii) less geographically limitation as spent batteries are spread worldwide (mostly in US, Europe, and BRICS) [4,17].

Recycling of Li-ion batteries has been largely studied [5,18–23], but challenges remain. Hydrometallurgical route is being considered due to their flexibility to recycle different types of batteries [24–26] and products including cathode resynthesis [27], and low environmental impact [14,28]. Before chemical steps, physical processing is capable of recovering the external structure (case), plastic (separators), and electron collectors (Al and mainly Cu foils) [29]. In comparison to pyrometallurgy, on the other hand, high energy is needed with larger emissions of greenhouse gases, and Li is lost in slag phase; high pure products are obtained after hydrometallurgical processing [30]. In direct recycling, excessive dependency on manual labor is the major challenge, especially mechanical disassembly due to the large variety of batteries in the market; moreover, this technology is still in laboratory scale and does not meet industrial requirements [31]. For this reason, the choice of hydrometallurgical processing in this study is focused on lower environmental impact (than pyrometallurgy) and fast upscaling (than direct recycling).

After acid leaching (e.g. H_2SO_4), the leach solution of Ni-rich batteries (NMC and NCA cathode batteries) contain high concentration of Li, Ni, Co and Mn from cathode material, Al and Cu from foils, and Fe as contaminant [24–26]. Traditional processes use solvent extraction for separation of valuable elements (Li, Ni, Co and Mn), but it has been

* Corresponding author at: Department of Chemical Engineering, Norwegian University of Science and Technology, Trondheim, Norway.
E-mail address: amilton.b.b.junior@ntnu.no (A.B. Botelho Junior).

https://doi.org/10.1016/j.cej.2026.173667
Received 28 November 2025; Received in revised form 29 January 2026; Accepted 31 January 2026
Available online 4 February 2026

shown in literature that losses of Co in the presence of Mn. Solvent extraction using bis(2-ethyl-hexyl) phosphoric acid organic solvent (D2EHPA) can be used to obtain 99.6% of Mn sulfate but requires many steps of extraction/stripping (up to 7) [32,33], and these several steps result in losses of valuable metals, mostly Co [24]. However, as demonstrated in previous study of our group, successfully separation of Co, Ni and Li by solvent extraction is performed in the lack of Mn ions in solution and does not support large different feed streams or distinguish compositions [26] which limit limits the recycling of different types of Ni-rich batteries. Alternatively, our group used ozone precipitation for selective separation of Mn with purity of 96% as oxide for battery or steel industries [34].

In this study, we propose a flexible hydrometallurgical route for recycling Ni-rich Li-ion batteries to meet the sustainable mining goals [16,35,36]. Inorganic and organic acids have been previously studied [37–41] and also by our group [24,26,42], and here it is demonstrated the possibility to use H_2SO_4 or H_3PO_4 as costly and environmental alternatives [21,43,44]. In separation and purification steps, ion exchange resins were evaluated for selective separation due to the selectivity for Ni and Co [45].

Beyond the inherent challenges of selectively separating Co and Ni, the adsorption step in ion-exchange systems requires a detailed understanding of equilibrium behavior and the actual retention capacity of the resins under different operational conditions. In this context, a multivariate evaluation of the adsorptive performance became necessary, one that could simultaneously account for the affinity between the metal ions and the adsorbent materials, as well as the hydrodynamic effects arising from changes in flow rate and bed-saturation dynamics. To this end, breakthrough experiments were employed—a methodology that enables monitoring the temporal evolution of the effluent concentration as the system approaches equilibrium, making it possible to calculate, through integral mass balances, the amount of each species accumulated in the bed and the corresponding equilibrium solid-phase concentrations.

Life cycle assessment (LCA) was important to quantify the environmental impact of the recycling process [43,44] and stablish a Ni-rich battery recycling process. The flexibility of the flowchart proposal allows the production of hydroxides, carbonate, oxalates, and oxides for several types of markets, such as batteries, chemicals, and steel. Future improvements could be performed to produce metals (e.g., electrowinning). Our research objectives were: i) compare inorganic acids (H_2SO_4, H_3PO_4) in leaching; ii) evaluate Mn precipitation by ozone; iii) study the selective separation of Ni and Co by ion exchange chelating resins and multivariate analysis; iv) environmental impact assessment of the flowchart proposed.

2. Materials and methods

2.1. Characterization and physical treatment

Cylindrical batteries (20 units, 903.2 g in total) were first discharged mechanically with Ni—Cr wires resistance until 0 V at room temperature (~25 °C) to avoid accidents and explosions. Further, one cell was manually dismantled for characterization, while others were used for physical treatment and leaching experiments. In characterization, the cell was opened with a precision cutter at 875 rpm, and the materials were separated in external structure (also known as case), cathode + Al foil, anode + Cu foil, and separator. Electrolyte characterization is out of our scope, and volatile compounds were removed as the parts were dried at 60 °C for 24 h. Cathode and anode were analyzed in XRD and digested in aqua regia for chemical analysis in ICP-OES, AAS and EDXRF. Separator was analyzed in FTIR and DSC [15]. Analytical procedures are detailed in Supplementary Material.

In black mass preparation, we used a procedure stablished in our group including all types of batteries (pouch, cylindrical, and prismatic) [25,26,46], and further improved for better separation of materials [29]. In both cases, materials recovery reached over 95%. The first grinding was performed with batteries discharged in a knife mill with 5.4 mm grid, the resulting material was dried in a fume hood for 24 h and later a sieving step to remove external structure and separator. The second grinding was performed Willey-type mill followed by sieving to remove remaining case and plastic and including Cu foil. Resulting material was used for leaching experiments.

2.2. Leaching experiments

Experiments were performed in 200 mL three-necked glass reactors on a heating plate under magnetic stirring, with condenser and thermometer were coupled to the reactor (Fig. S1). The solutions used as leaching agents were H_2SO_4 (98%) and H_3PO_4 (85%) prepared with ultrapure water. The effect of solid-liquid (S/L) ratio, acid concentration, temperature and time were evaluated (Table S1). After leaching, the solution was filtered, and samples were diluted (HNO_3 3%) for chemical analysis in AAS and EDXRF. Leaching efficiency was calculated as shown in Eq. 1, where C_e is the concentration (mg/L) of the element analyzed, $D.f.$ is the dilution factor, V_L is the volume of the leaching liquor (L), and m_S is the mass of the sample (mg) used on the experiment multiplied by P_{el}, which is the percentage of the element present in black mass.

$$Percentage\ of\ leaching = \frac{C_e \times D.f. \times V_L}{m_S \times P_{el}} \times 100 \quad (1)$$

2.3. Separation and purification experiments

After leaching, different techniques were evaluated for separation and purification to obtain critical metals products. The main reasons to test stablished hydrometallurgical techniques are, first, for fast upscaling and flexibility into different types of spent cathode materials (i.e., NMCs, LCO, NCA LMO) into a flexible process, and second to use consolidate data for LCA and optimization. We tested ozone precipitation, solvent extraction, ion exchange chelating resins, and alkali/oxalic precipitation. Parameters evaluated are detailed in Table S2. Solutions composition was determined in AAS, EDXRF and flame photometer.

Ozone precipitation experiments were carried out for Mn precipitation, as reported in our previous work [34,47] including systematic parameters evaluation in NMC cathode leaching solution such as influence of pH, ozone concentration, reaction temperature. Although previously reported, our goal was to demonstrate the use of this technique in different leaching compositions and later develop a flexible system for different leach compositions. Experiments were performed in 500 mL three-necked glass reactors under magnetic stirring with the leach solution with ozone addition coupled to the reactor. Ozone was produced in-situ (lab), which represents a great advantage for upscaling, where oxygen (99.5% purity) was added controlled by a mass flow feeding to an ozone generator, and later passes through a gas washing bottle before going to the reactor by a porous tip that forms bubbles. The gas released out the solution was eliminated using a KI solution of 5% (*w/v*). After experiment, solution was filtrated, and the precipitate was dried at 60 °C for 24 h for XRD analysis. Ozone concentration was determined as detailed reported in literature [34,47].

Solvent extraction experiments were performed in batch for 15 min at 25 °C and aqueous/organic (A/O) ratio 1/1 diluted in kerosene, and we studied two different extractants (Cyanex 272 10%*v*/v – bis (2,4,4-trimethyl- pentyl) phosphinic acid, and D2EHPA 5%v/v - di-(2- ethylhexyl)phosphoric acid) and the effect of pH [26,48,49]. Ion exchange chelating resins experiments were performed in batch and column (continuous), and two resins (Dowex M4195 and Lewatit TP 220) with the same functional group (bis-picolylamine) were evaluated. Before experiments, resins were washed with HCl 4.0 mol/L and ultrapure water and later dried at 60 °C for 24 h before experiments. Batch experiments were performed with 1 g of resin and 50 mL solution in shaker

(200 rpm) for 2 h. Columns experiments were performed to simulate a continuous process in a glass column 30 cm long (bed height) and with an internal diameter of 1 cm, whose resin bed volume was 10 mL (bulk density: Lewatit TP 220–690 g/L; Dowex M4195 – 673 g/L).

Precipitation experiments were performed with NaOH (97%) for separation of Al as we previously proposed [26] and $H_2C_2O_4$ (99%) for separation of Ni and Co [42,50]. For the experiments, 50 mL of solution was stirred (magnetic) in a 120 mL beaker under pH and temperature control. The precipitated was washed with water at the same pH of the experiment to avoid losses by dissolution and dried at 60 °C for 24 h before analysis. The resulting solution contained only Li in sulfate solution, and anions were removed by $Ca(OH)_2$ only to further produce LiOH by crystallization. It is from our understanding that other techniques should be used for sulfate separation for acid recovery, such as electrodialysis [51,52], but here this step was out of scope, and it is suggested in future studies. Crystallization of Li sulfate was previously reported by our group [26].

2.4. Multivariate analysis

In the studies, it was observed that there was a possibility for optimizing selective ion exchange separation between Ni and Co over Al and Li. Our choice for optimizing ion exchange separation was due to i) strong selective separation of valuable metals (Ni and Co); ii) high concentration of metals and consequently short breakthrough curves; iii) determine process parameters for upscaling. Description of multivariate analysis model validation is depicted in Supplementary Material.

In the process, the equilibrium adsorbate concentration (metallic ions = Ni and Co) in the solid phase (chelating resin = Dowex M4195 and Lewatit TP 220) is determined from a series of breakthrough experiments in which the column is successively exposed to different feed concentrations. In each step, the column is first saturated with the solution corresponding to the previous steady state; then the feed is switched to a new concentration ($C_{in,i}$) and kept constant until a new steady state is reached. Once this new steady state is established, the liquid and solid phase compositions represent an equilibrium point of the multicomponent adsorption isotherm. From the breakthrough profile obtained during the transition between two consecutive steady states, a global mass balance is used to compute the variation (Eq. 2) in the number of moles of component (i) accumulated in the bed (both in the void space and in the solid phase) [53], where (Q) is the volumetric flow rate, t_{exp} is the total time considered for the breakthrough step, $C_{in,i}$ is the inlet concentration of component (i), and $C_{out,i}$ is its outlet concentration as a function of time.

$$\Delta n_i = Q \int_0^{t_{exp}} \left(C_{in,i} - C_{out,i)} dt \right. \tag{2}$$

The quantity Δn_i is then related to the fluid and solid concentrations through a volume-averaged balance (Eq. 3) that accounts for the bed porosity ε_b, the intraparticle porosity ε_p, and the total bed volume (V), where $C_{o,i}$ is the liquid concentration of component (i) at the previous steady state and $q_i(C)$ is the adsorbed concentration in equilibrium with a given liquid concentration (C).

$$\frac{\Delta n_i}{V} = \left[\varepsilon_b + (1-\varepsilon_b)\varepsilon_p\right]\left(C_{in,i} - C_{0,i}\right) + (1-\varepsilon_b)\left(1-\varepsilon_p\right)\left[q_i\left(C_{in,i}\right) - q_i\left(C_{0,i}\right)\right] \tag{3}$$

$$q_i\left(C_{in,i}\right) = q_i\left(C_{0,i}\right) + \frac{\frac{\Delta n_i}{V} - \left[\varepsilon_b + (1-\varepsilon_b)\varepsilon_p\right]\left(C_{in,i} - C_{0,i}\right)}{(1-\varepsilon_b)\left(1-\varepsilon_p\right)} \tag{4}$$

Thus, for each feed-concentration step and for each component, the integration of the breakthrough curve provides Δn_i, and the volume-averaged balance allows the calculation of the new equilibrium adsorbed concentration $q_i\left(C_{in,i}\right)$ (Eq. 4). The resulting set of experimental points $\left(C_{in,i}, q_i\left(C_{in,i}\right)\right)$. can then be used to estimate the parameters of competitive adsorption isotherm models (e.g., the competitive Langmuir isotherm) and to validate the proposed adsorption model [53].

2.5. Flowchart proposal and life cycle assessment

A flowchart for recycling of NMC811 was proposed based on laboratory experiments. Upscaling data was not considered in our analysis. The mass balance was calculated considering the best conditions from physical treatment (903,2 g of spent cylindrical cells) to metallic products. Boundary limits of LCA were determined with SimaPro 9.5.0.1 software was used for the LCA with the calculation method ReCiPe 2016 v1.1 midpoint, Hierarchist version [20,54]. The system was considered limited to the recycling process, with expansions to consider the effects of waste treatment and avoided products. Battery production, the use and collection of discarded LIBs, and other lifecycle stages were not considered.

Life cycle inventory (ReCiPe software) was calculated and analyzed following environmental impact categories: Global Warming Potential (GWP), PED (Primary Energy Demand), and Mineral Resources Scarcity. Ecoinvent v3.6 database was used which includes information on materials and energy sources. Brazilian low-voltage energy matrix of the Southeast region was considered for the analysis considering the 2023 National Energy Balance (BEN). Both material inputs and outputs were obtained based on the global production values available in the database. A baseline scenario was created to determine the results using SimaPro software as an attributional model (one product as the main one – LiOH), instead of a consequential and multi-element model, considering several main products.

3. Results and discussions

3.1. Sample characterization and physical treatment

After being discharged (0 V), the characterization was proceeded open the cell manually and separating the materials for characterization (Table 1). Volatile electrolyte represents 15.8% of the cell battery, while polymeric separator (polypropylene – PP) represents 1.1%. Cylindrical external structure is an Al alloy. Cathode ($LiNiMnCoO_2$ as NMC811, 41.5%) and anode (graphite, 26.5%) represent 68% of the cell battery and the most valuable and interesting for recycling, mainly the metallic elements. The potential economic value for this battery is 6000–11,000 USD/ton to be obtained by recycling [15,25] which varies according to the commodity prices [1,8,55–57]. Our physical treatment was performed by grinding followed by particle size separation in two steps. In this processes, losses were graphite (powder) and electrolyte (volatile) reaching 5.2% considering the whole physical process. In the first step, up to 44% of both separator and external structure were separated, and in the second step a concentrated material removed remained external structure and polymeric fraction, but also Al and Cu foils. Resulting material (below 2.0 mm, Table 1) still contains Al and Cu foils due to strong bond with cathode and anode, respectively [15]. However, for acid leaching, Al foil works as a reducing agent reducing the costs and environmental impact of the reaction [14,26].

3.2. Leaching experiments

The goal of this chapter was to make a comparison of two different inorganic acids (H_2SO_4 and H_3PO_4) of a NMC811 battery black mass without the use reducing agent. Details about H_2SO_4 leaching are reported elsewhere [25], and here we depict the leaching data for H_3PO_4. Acid leaching kinetics of NMC811 reach the equilibrium after 2 h in both cases. No reducing agent was added in the experiments due to the presence of Al foil particles working as reducing agent generating Al ions (+3). The black mass has d10, d50 and d90 equals to 6.5 μm, 25.7 μm

Table 1
Materials and elementary (cathode and anode) composition of the cylindrical battery [15,25].

Materials in the cell battery	Composition	Elements (cathode and anode) in the cell battery	Composition	Elements in the black mass	Composition
Cathode	41.5% (16.7 g)	Ni	15.0%	Ni	16.2%
Anode	26.5% (10.6 g)	Mn	2.9%	Mn	5.6%
Separator	1.1% (1.0 g)	Co	3.0%	Co	4.5%
External structure	15.1% (6.0 g)	Li	2.0%	Li	3.7%
Electrolyte	15.8% (6.2 g)	Al	3.1%	Al	6.3%
		Cu	11.8%	Cu	13.6%
		C	11.2%	C	22.5%
Battery cell (total)	100% (40.5 g)	Battery cell (total)	49.0%		

and 158.9 μm, respectively.

Differences were observed among these acids related to the chemical reaction (Eqs. 5 and 6). For instance, H_3PO_4 leaching requires larger stoichiometric ratio than H_2SO_4 for complete reaction (100% of cathode leaching) – 168% and 142%, respectively (Fig. 1a,b) for S/L ratio 1/10. Indeed, the literature reports that reducing agents as H_2O_2 increases kinetic leaching mostly due to the conversion of Co(III) into Co(II) but largely increases the environmental and economic impacts [14]. For instance, in another study of our group, reducing agent may represent 15% of the costs in leaching reaction of NCA battery [26]. Considering a battery recycling process that the feed material can be a mix of different cathode materials, the presence of Al will be observed because of NCA-cathode. So, Al ions in solution will be found anyway.

$$20\,LiNi_{0.8}Mn_{0.1}Co_{0.1}O_{2\,(s)} + 30\,H_2SO_{4\,(aq)} \rightleftharpoons 16NiSO_{4\,(aq)} + 2CoSO_{4\,(aq)} + 2MnSO_{4\,(aq)} + 10Li_2SO_{4\,(aq)} + 30\,H_2O_{(l)} + 5\,O_{2\,(g)} \quad (5)$$

$$60\,LiNi_{0.8}Mn_{0.1}Co_{0.1}O_{2\,(s)} + 60\,H_3PO_{4\,(aq)} \rightleftharpoons 16\,Ni_3(PO_4)_{2\,(aq)} + 2\,Mn_3(PO_4)_{2\,(aq)} + 2\,Co_3(PO_4)_{2\,(aq)} + 20\,Li_3PO_{4\,(aq)} + 90\,H_2O_{(l)} + 15\,O_{2\,(g)} \quad (6)$$

Differences were also observed varying the acid concentration (Fig. 1c,d). It occurs not because of the amount of protons (H^+) that each acid has, but due to acid dissociation in water is not complete. As a consequence, H_2SO_4 leaching of Ni and Co increased from 44 to 45% (0.5 mol/L) to 100% (1.0 mol/L), and Mn increased from 43% (0.5 mol/L) to 95% (1.0 mol/L), while H_3PO_4 leaching of Ni and Co increased from 25 to 30% (0.5 mol/L) to 100% (2.0 mol/L), and Mn increased from 29% (0.5 mol/L) to 100% (2.0 mol/L). Li leaching followed a similar behavior, and highlighted by two important factors – first, Li is not easier to be leached but also present part of electrolyte composition as fluoride salts after organic phase evaporation in physical processing; and second, Li sulfate is more soluble (no k_{sp} because high solubility in water) than phosphate ($k_{sp} = 2.4 \times 10^{-11}$) which helps on leaching efficiency.

Leaching efficiency increasing temperature (Fig. 1e,f) demonstrated that the reaction is endothermic as the efficiency increases with the temperature. The highest efficiency (close to 100% in 2 h) in H_2SO_4 leaching was achieved as S/L ratio 1/10, 1.0 mol/L at 90 °C, while for H_3PO_4 leaching it was achieved with /L ratio 1/10, 2.0 mol/L at 90 °C. Our preliminary economic analysis (considering only reagents used for the reaction) has demonstrated that H_3PO_4 leaching is 68.7% more expensive than H_2SO_4 leaching due to the higher acid concentration required and cost. Sulfuric leaching still remains the best option in battery recycling. After reaction, the leaching residue (solid phase) is highly concentrated in graphite with 96.6% purity, and minor elements are unreacted cathode materials (Al - 0.38%, Ni - 1.05%, Co - 0.38%, Mn - 0.32%), case (Fe - 0.05%) and electrolyte (Cl - 1.98%). Further acid treatment is suggested to increase purity for future applications [58].

3.3. Separation and purification methods

Leaching solution contains a challenge that was not found in classical metallurgical process (Table 2) which is the high concentration of valuable metallic ions. For instance, solvent extraction is commonly used for separation in hydrometallurgical processing after leaching, but NMC processing result in losses of Mn and Co throughout the process

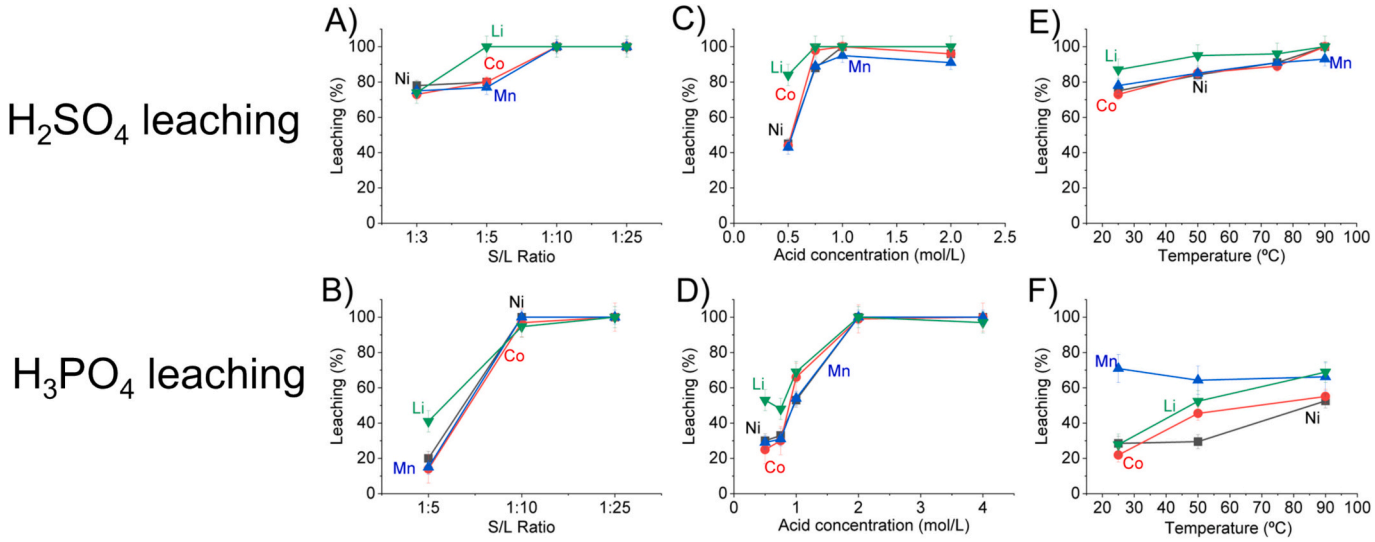

Fig. 1. Leaching efficiency of Li, Ni, Co, and Mn from NMC811 battery black mass during 2 h of reaction varying the solid/liquid (S/L) ratio at 90 °C with 2 mol/L of a) H_2SO_4 and b) H_3PO_4, concentration of c) H_2SO_4 and d) H_3PO_4 at 90 °C and S/L ratio 1/10, and temperature with S/L ratio 1/10 and 2 mol/L of e) H_2SO_4 and f) H_3PO_4.

Table 2
Composition of the H_2SO_4 leaching solution of NMC811 battery black mass at S/L ratio 1/10, 1.0 mol/L at 90 °C for 2 h.

Elements	Concentration (g/L)
Ni	18.08
Mn	5.78
Co	5.03
Li	4.10
Al	3.33

due to the interaction of the ions. As Locati et al. (2024) demonstrated, separation using D2EHPA reached 99% of Mn extraction but losses of Co were observed around 40–80% although the authors reported a 3% co-extraction in a continuous process [32]. Similar finds were observed in an in-depth analysis of solvent extraction for NMC recycling [24]. In Vieceli et al. (2023)' work, the authors highlighted that solvent extraction process is performed without problems after Mn removal [59], as we reported before [26]. As alternative, our group previously developed a system for Mn precipitation using ozone injection [34], and therefore we evaluated the battery recycling flowchart of the present work, also due to the discussion about environmental impact (LCA) and process optimization.

Based on our previous work, preliminary experiments were carried out at pH 2.0, 3.0 L/min O_2 (65.7 mg/min of O_3) and at 25 °C over time. Mn precipitation increased from 33.9% (3 h) to 56.5% (5 h) and 98.9% (10*h*). The pH is pivotal for both Mn precipitation and selectivity; according to the Pourbaix Diagram, in the NMC-based leaching solution, selective precipitation of Mn occurs at pH 0.5–2.0 in redox 1.2–1.7, while the increase of temperature has no substantial effect on selective precipitation [60]. Moreover, during the process, the pH decreases over time since ozone acts as a Lewis acid and reached pH 0.84 and redox potential 1.253 V after 10 h experiment. However, co-precipitation of Co reached 35.5%. Based on authors' knowledge, it occurs due to the excess of ozone added in the solution, where Co precipitates after Mn precipitation. It is corroborated by Ichlas et al. (2020), where Co precipitation increases from 30% (15 min) to 98% (1 h) as Mn was entirely precipitated (in 15 min); after all Co precipitation, Ni precipitation increased [60]. As a conclusion, it can be inferred that ozone has an order of selectivity for separation in acid (sulfate) conditions is Mn > Co > Ni. In our experiments, the precipitation of Ni, Al and Li was not detected.

At pH 0.5, the highest selectivity for Mn precipitation was observed (Fig. 2a). The increase of pH promoted the precipitation of Co; contrasting to previous study [34], the solution (Table 2) contains higher concentration of Co requiring lower pH (0.5) for better selectivity for Mn; moreover, all Mn was precipitated in 5 h (Fig. 2b) with low co-precipitation of Co (2.9%), which is a half of time. We also observed that 3.0 L/min was in excess, and co-precipitation of Co was reduced until 1.8% with 0.2 L/min O_2 (which was converted into ozone – 4.4 mg/min O_3). The advantage of ozone precipitation after leaching reaction is due to the minor pH adjustment and high selective precipitation of Mn that can be used for cathode synthesis or steel production. The energy required to generate 1 kg of ozone can be considered as 16.4kWh [47], so in this experiment it was consumed 21.7 Wh to generate the ozone needed for the lab experiment. Future studies can aim at continuous precipitation process for Mn precipitation to optimize the reaction time. Our previous study [34] also demonstrated that bubble sizes affect the precipitation kinetic, which could be also evaluated in the future.

After Mn precipitation, two ion exchange separation were evaluated: solvent extraction (liquid-liquid) and ion exchange resins (solid-liquid). The motivation was based on technical alternatives from previous studies reported in literature [26,32,59,61]. In a solution containing Ni, Co, Li and Al, no selectivity was observed in extraction by Cyanex 272 (Fig. S2) in a pH range 1.0–3.5 due to the selectivity for this extractant keeping between 70 and 85% extraction efficiency to all pH values studies. For instance, theoretical extraction of Al ions in sulfate media would increase from pH 1.0 to 3.0 but also increases for Co from pH 1.7 to 5.0, while extraction of Mn increases in a pH range 3.2–5.0; extraction of Ni occurs in pH over 6.0 [62]. The selectivity for Al may increase at pH 0.5 in higher organic concentration (20%) but several extraction steps will be required resulting in losses of co-ions (mostly Mn and Co) throughout the steps [63,64]. Literature reports the use of Cyanex 272 for impurities removal (as Mg and Ca) from leaching solution [65,66]. High selectivity was achieved by Cyanex 272 after Al removal [48]. On the other hand, D2EHPA was selective for Al and Li (25% for both) without co-extraction of Ni and Co (D2EHPA 5%*v*/v, A/O 1/1, 25 °C for 15 min). It opens as alternative for future application but still requires multiple steps.

We evaluated the use of ion exchange chelating resins in batch and column (continuous) with two commercial resins (Dowex M4195 and Lewatit TP 220). Both resins were tested due to the selectivity of the functional groups as the following order Ni > Co > Mn > Al (considering only metals present in the solution studied) [67–69]. In batch experiments varying the pH (Table S3), adsorption of Li and Al was not observed. Ni and Co separation achieved the maximum adsorption (23.1%–26.0% and 15.4%–21.1% respectively) at pH 3.0 mostly due to the deprotonation of functional groups and less competition between H^+ with the metallic ions [70,71]. Differences among the ion exchange chelating resins were not related to the functional group but due to structural and physicochemical factors of the resin matrix (polymer matrix and crosslinking degree) [72,73]. Higher adsorption efficiencies were found for Lewatit TP 220 (24.9%–26.0% for Ni and 10.4%–15.4% for Co at pH 1.0–3.0).

Column experiments were carried out to simulate a continuous process (Fig. S3), where no adsorption of Al and Li were observed. Adsorption of Ni and Co increases similarly where the resins were slightly more selective for Ni than Co and reaching the breakthrough point at the same time. The resins followed similar behavior achieving

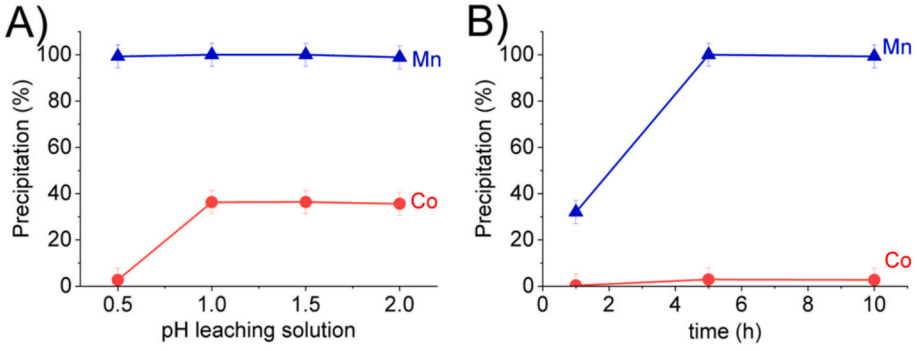

Fig. 2. Precipitation efficiency for Mn and Co from leaching solution of NMC811 black mass a) varying the pH of the leach solution at 3.0 L/min O_2 and at 25 °C for 10 h; and b) varying the time at pH 0.5, 3.0 L/min O_2 and at 25 °C.

fast the breakthrough point and saturating in 50-200 min with a slight selectivity for Co over Ni due to the different concentrations of ions (Ni-18.0 g/L and Co-5.03 g/L). However, we observed that Dowex M4195 resin reached 28.4% adsorption of Ni and 25.2% adsorption of Co, which could be further removed from the resin (elution process) to obtain a Ni—Co concentrated material. On the other hand, Lewatit TP 220 reached 4.1% of Ni adsorption and close to 0% adsorption of Co after about 7 h experiment. As observed in the breakthrough curves (Fig. S3b, d,f), the resin rapidly reached the equilibrium on Co adsorption and later released them for adsorption of Ni ions due to higher concentration competing for the functional groups. Similar results were previously reported for mining processing and e-wastes [45,74,75]. Ion exchange chelating resins seem to be an interesting approach for Ni—Co separation from Al and Li, but requiring several columns in series and parallel, and high concentration of ions in a battery recycling leaching solution is a drawback.

In our previous work for NCA recycling process [26], we demonstrated that Al removal from the leaching solution is possible at pH 5.0 and 80 °C, where these ions were leached from cathode and foil material. The advantage of this step is that Al ions will be found in both NMC and NCA leaching solution, and the precipitation step will be necessary for a flexible process to recycle all types of Li-ion batteries. All Al was precipitated with losses of 2.9% of Ni, and a washing step (H_2O pH 5.0) was important to reduce co-precipitation of valuable metals. The Al hydroxide has 97% purity.

After Mn and Al precipitation, the solution contains high concentration of Ni, Co and Li. Precipitating agents NaOH and oxalic acid ($C_2H_2O_4$) were studied for Co and Ni precipitation. No losses were observed using NaOH (Table 3) reaching 97% precipitation efficiency. Mixed hydroxide precipitate (Ni—Co) is commonly used in Ni and Co processing but mostly using MgO as precipitating agent [60,76] and we avoided it to reduce potential contamination of Li product (next step). However, the use of MgO is interesting for future studies in battery recycling since it is further produced as sulfate ($MgSO_4$) and then reacted thermically to obtain again MgO and generate H_2SO_4 [77]. Also, Li losses were not observed as precipitates in high pH as hydroxide and mostly obtained as carbonate due to solubility [78]. In $C_2H_2O_4$ precipitation (Table S4), losses of Li were observed (3.5%–5.1%) due to high ionic strength decreasing Li-oxalate solubility in sulfate solution resulting in co-precipitation [40,50,79]. In our case, the increase of temperature did not reduced Li losses.

For Li crystallization, sulfate ions were removed by $Ca(OH)_2$ as $CaSO_4$. For future studies, we suggest the use of electrodialysis for LiOH and SO_4^{-2} separation [51,52,80,81], also to avoid losses in the solid phase (Table S5, 11.9%–16.1%). Another approach is crystallization as $LiSO_4$ [26] that reached 78.8% efficiency.

3.4. Multivariate analysis

Breakthrough experiments were carried out for both Co and Ni by Dowex M4195 and Lewatit TP 220. As observed (Fig. S3), high selective separation of valuable metals was obtained; however, due to high concentration of metallic ions (Table 2), the breakthrough curve is rapidly reached, and optimization can help for data processing and upscaling future battery recycling processes.

To better interpret these results and to support decision making and upscaling for future battery-recycling applications, a multivariate analysis was conducted, enabling the simultaneous assessment of resin type, metal species, and hydrodynamic conditions and their combined influence on adsorption behavior.

Table 3
Precipitation efficiency of Ni and Co varying the pH by NaOH at 80 °C for 30 min.

pH	Ni	Co
7.5	34.6%	36.0%
8.0	90.7%	91.9%
8.5	97.4%	97.1%

Effluent concentration increases from nearly zero to values close to $\boldsymbol{C_{in}}$ for both resins indicating the progressive saturation (Fig. 3 and Fig. 4). At lower flow rates, the breakthrough is more gradual, and the shaded area is larger, reflecting a higher overall uptake of metallic ions (Ni and Co), whereas at higher flow rates the curves become steeper and the available contact time decreases, resulting in smaller areas and therefore lower values of $\boldsymbol{\Delta n_i}$ and $\boldsymbol{q_i}(\boldsymbol{C_{in,i}})$.

Since the inlet concentrations of Co and Ni are essentially the same for all runs (Table 4 for Dowex M4195 and Table 5 for Lewatit TP 220), the differences observed in $\boldsymbol{\Delta n}$, $\boldsymbol{\Delta n/V_{bed}}$, and $\boldsymbol{q_i}(\boldsymbol{C_{in}})$ mainly reflect the effects of the flow rate and the affinity of the resin for each ion. At the lowest flow rate (3BV/h), both metals exhibit higher adsorption compared to the highest flow rate (9BV/h), as indicated by the larger values of $\boldsymbol{\Delta n}$ and $\boldsymbol{\Delta n/V_{bed}}$, which is consistent with the longer contact time available for mass transfer. Ni systematically shows higher $\boldsymbol{\Delta n/V_{bed}}$ and $\boldsymbol{q_i}(\boldsymbol{C_{in}})$values, revealing a stronger interaction with the Dowex M4195 and a higher equilibrium capacity. At 3BV/h, for example, $\boldsymbol{q_i}(\boldsymbol{C_{in}})$for Ni is in the order of $\boldsymbol{1.69 \times 10^4}\,\mathrm{mol/m^3_{solid}}$ of solid, more than eight-fold the value obtained for Co ($\sim \boldsymbol{2.0 \times 10^3}\,\mathrm{mol/m^3_{solid}}$). As the flow rate increases to 6 and 9BV/h, both metals experience a reduction in $\boldsymbol{\Delta n}$ and $\boldsymbol{q_i}(\boldsymbol{C_{in}})$, with the effect being particularly pronounced for Co at 9BV/h, where the equilibrium capacity drops to values below $\boldsymbol{8.9 \times 10^2}\,\mathrm{mol/m^3_{solid}}$. Overall, the table quantitatively confirms the trends observed in the breakthrough curves: lower flow rates and the Ni–Dowex M4195 pair favor higher adsorption capacities, and these data constitute the basis for the subsequent estimation of the competitive isotherm parameters.

There are consistent trends regarding the effect of resin (even with the same functional group bis-picolylamine), flow rate, and metallic ion on the adsorption performance, where Dowex M4195 exhibits systematically higher equilibrium capacities than Lewatit TP 220 for both Ni and Co. For example, at 3BV/h the equilibrium solid-phase concentration for Co on Dowex M4195 is on the order of $2.0 \times 10^3\,\mathrm{mol/m^3_{solid}}$, whereas for Lewatit TP 220 it is below $4.0 \times 10^2\,\mathrm{mol/m^3_{solid}}$; for Ni, the difference is also marked with about $1.69 \times 10^4\,\mathrm{mol/m^3_{solid}}$ on Dowex M4195 versus $7.18 \times 10^3\,\mathrm{mol/m^3_{solid}}$ on Lewatit TP 220. This trend persists at 6 and 9BV/h, indicating that Dowex M4195 has a higher adsorption capacity overall and therefore a stronger affinity for both Co and Ni under the conditions studied.

Differences in the chelating resins were observed although same functional group are present in both resins (bis-picolylamine). In our modeling, we considered the same parameters including porosity and particle size distribution, and results were in accordance with experimental data. On the other hand, the difference in metallic ions adsorption might be related to physical reactions and not by chemistry. Our hypothesis is that Dowex M4195 has slightly lower bead size than Lewatit TP 220 [82], and this hypothesis is in accordance with Wesselborg et al. (2024) which observed differences in metallic ions adsorption in battery recycling process by Lewatit TP 260 and Lewatit MDS TP 260 (both with aminomethylphosphonic acid functional group) where smaller resin beads prevented early breakthroughs, allowing operation at increased volume flowrates [45].

In addition, lower flow rates generally favor adsorption by Dowex M4195. Values of $q_i(C_{in})$ for Co are similar and relatively high ($\approx 2.0 \times 10^3\,\mathrm{mol/m^3_{solid}}$) at 3 and 6BV/h, while at 9BV/h the capacity drops to below $8.9 \times 10^2\,\mathrm{mol/m^3_{solid}}$. For Ni, the highest Dowex M4195 equilibrium capacity is obtained at 3BV/h ($\approx 1.69 \times 10^4\,\mathrm{mol/m^3_{solid}}$) and decreasing as the flow rate increases to 6 and 9BV/h, consistent with the longer contact time at lower flow rates that enhances mass transfer and allows the bed (resins) to approach equilibrium more closely. For Lewatit TP 220, Ni also shows its highest capacity at 3BV/h and a reduction

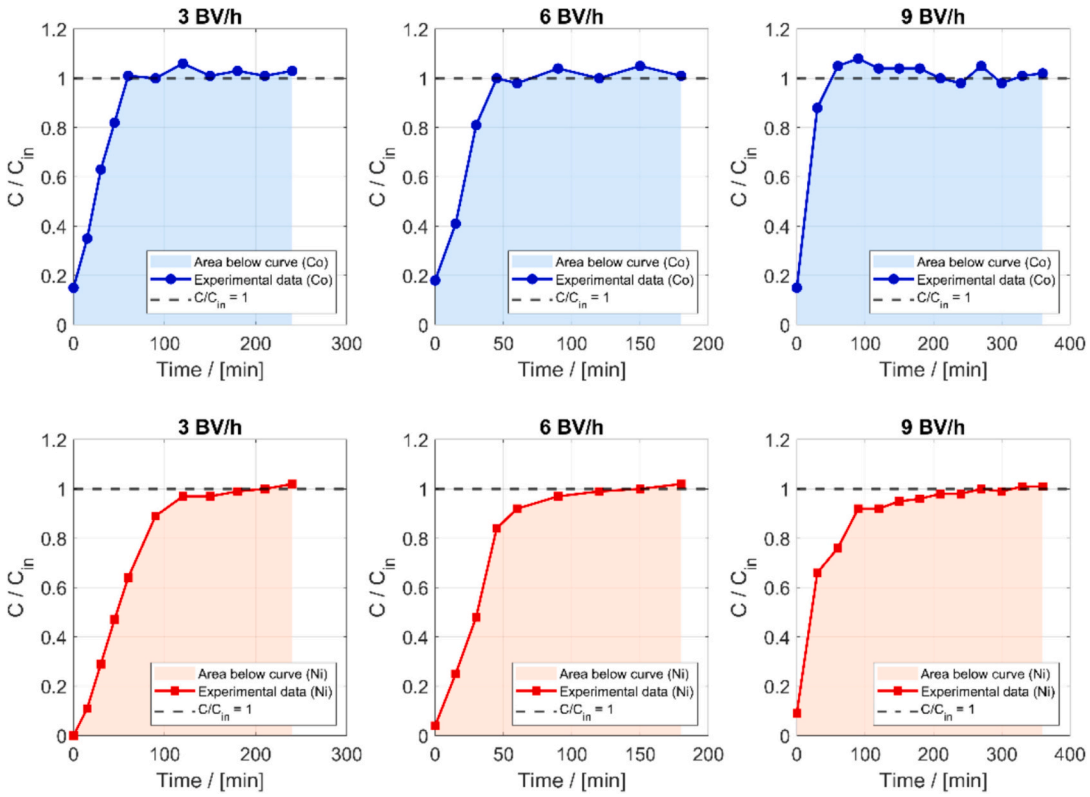

Fig. 3. Breakthrough curves of Co and Ni on Dowex M4195 at different flow rates (3, 6, and 9 BV/h). The symbols represent the experimental values of the dimensionless concentration C/C_{in} as a function of time and the shaded region under each curve highlights the area to calculate Δn_i.

at higher flow rates, whereas Co presents a milder trend with somewhat increasing capacities from 3 to 9BV/h. According to the calculations and modeling optimization, the flow rate 3BV/h was the most favorable flow rate for maximizing adsorption especially for Ni, which dominates the adsorption on both chelating resins. Similar conclusion regarding flow rates were observed for battery recycling [45] and Ni laterite processing [83–85].

Finally, comparing the metallic ions in column adsorption, Ni is clearly the strongly metallic ion adsorbed in all cases (chelating resin and flow rate). Ni reaches values more than twice (Dowex M4195) and five-fold (Lewatit TP 220) those of Co at 3BV/h and remain superior at 6 and 9BV/h (Fig. 5). The equilibrium capacity q_{eq} for Co and Ni (Fig. 6) shows that Dowex M4195 exhibits systematically higher capacities than Lewatit TP 220 at all flow rates, where the highest capacities are observed at the lowest flow rate (3 VL/h) and q_{eq} decreases as the flow rate increases to 6 and 9BV/h, reflecting the reduction in contact time between liquid and solid. Ni shows significantly larger q_{eq} values than Co, indicating a stronger affinity for both resins. These trends are consistent with the behavior observed in the breakthrough curves (Fig. S3) and with the quantitative analysis presented in the equilibrium tables.

Our experimental data and calculations determined that Dowex M4195 is the more efficient resin, and lower flow rates are generally more favorable for achieving higher adsorption capacities. High concentrations of Ni and Co ions (Ni 18.08 g/L, Co 5.03 g/L) lead to rapid penetration of resin, which requires complex operations and increases the complexity of the process. Based on our study, future studies may benefit and explore recycling of ions exchange resins and long-term operation for economic analysis.

3.5. Flowchart proposal and LCA

Based on lab experiments, we proposed a flowchart (Fig. 7a) for recycling NMC811-type Li-ion batteries. The mass balance was calculated and used for LCA discussion. Considering almost 1 kg of cylindrical cells, about 31.4% is separated in dismantling (milling and physical separation) corresponding to plastics, Cu and Al foils, and external structure. Most valuable products are cathode materials – MnO_2 (88.6 g / kg black mass), Ni—Co oxalate (734.4 g / kg black mass) or Ni-Co-hydroxide as mixed hydroxide (Fig. S4), $Al(OH)_2$ (38.9 g / kg black mass), and LiOH (128.9 g / kg black mass). Indeed, leaching without external reducing agent (e.g., H_2O_2) is dependent on amount of Al foils in black mass for acid leaching, which can be impacted by physical sorting efficiency [86]. As previously discussed (chapter 3.2), there is lower environmental and cost impacts avoiding the use of H_2O_2 as reducing agent, and the presence of Al ions in the leaching solution does not impact a flexible process that will leach together Al-bearing black mass as in LCA ($LiCoAlO_2$) cathode batteries [26]. However, the amount Al foils necessary is dependent on the composition of black mass. For instance, in our study, only 13.65 g of Al was leached for complete leaching of NMC cathode material in black mass which represents 49% leaching efficiency, and it corroborates with our previous studies for LFP [87], NMC [24] and LCA [26], and also corroborate in another study for LFP recycling [37]. Future recycling process can use these studies (including this manuscript) to define better conditions for acid leaching.

For application to other types of cathode materials, such as NCA and LCO, small modifications in the flowchart are necessary. For instance, in NCA battery recycling, the Mn precipitation step is not necessary, while requires more precipitation of Al (from cathode and foil) [26]. In LCO recycling, higher concentration of Co ions is present in leaching solution, and no presence of Ni ions results in a pure Co-oxalate product (99.2%) [42]. In general, process parameters will slightly change depending on the cathode type keeping the purification steps.

For LCA (Fig. 7b), we considered the following categories as most important for critical materials production from recycling: GWP which calculates the CO_2 generated in the process as kg-CO_2eq; PED which

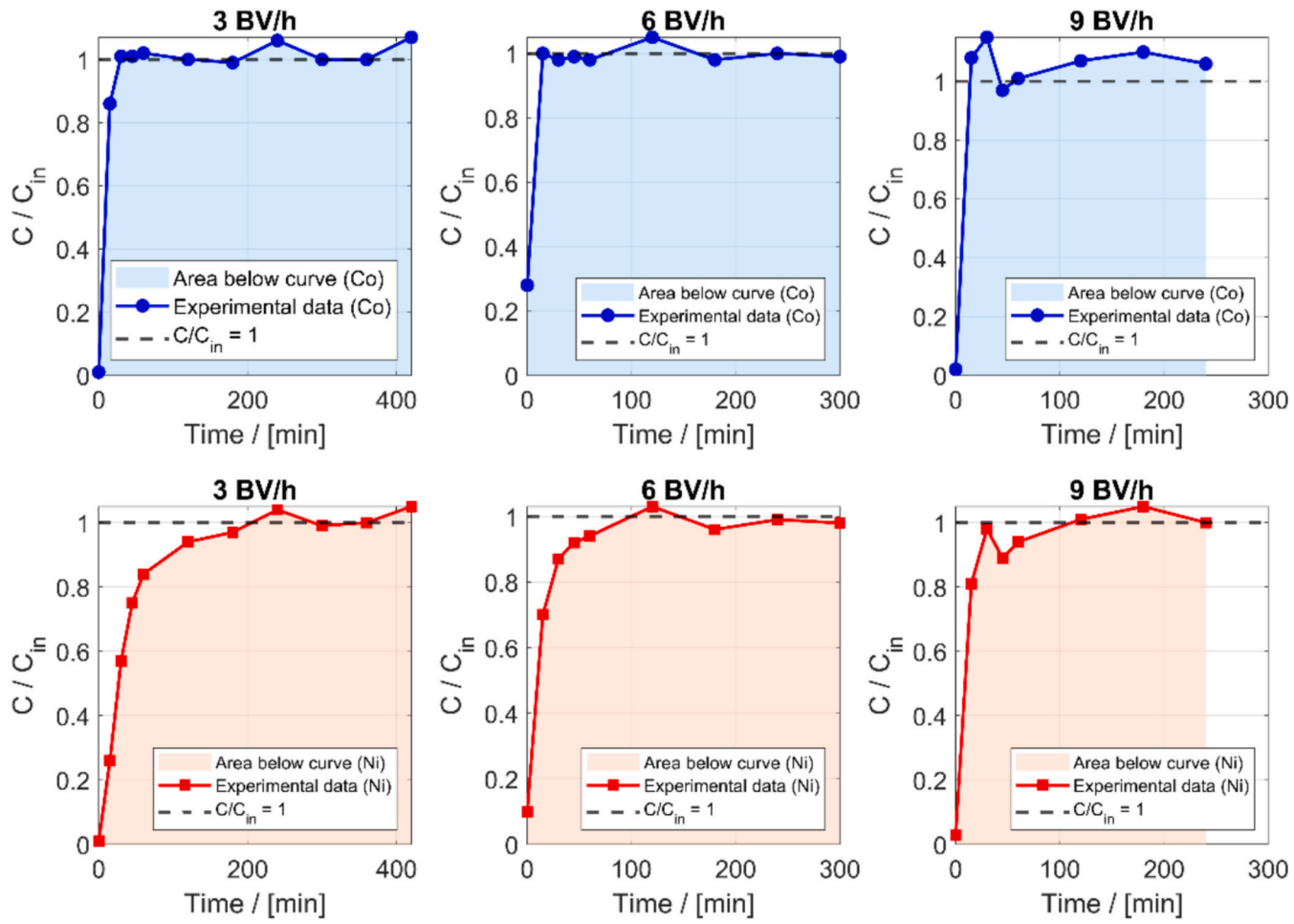

Fig. 4. Breakthrough curves of Co and Ni on Lewatit TP 220 at different flow rates (3, 6, and 9 BV/h). The symbols represent the experimental values of the dimensionless concentration $\boldsymbol{C/C_{in}}$ as a function of time and the shaded region under each curve highlights the area to calculate $\boldsymbol{\Delta n_i}$.

Table 4
Summary of breakthrough results for Co and Ni on Dowex M4195. Volumetric flow rate $\boldsymbol{Q}$, the inlet concentration $\boldsymbol{C}_{\text{in}}$, the total amount adsorbed in the column $\boldsymbol{\Delta n}$, the corresponding amount per unit bed volume $\boldsymbol{\Delta n/V}_{\text{bed}}$, and the equilibrium solid-phase concentration $\boldsymbol{q_i(C}_{\text{in}})$.

Metal	Flow rate	Q (m^3/s)	$C_{in}\left(\frac{mol}{m^3}\right)$	$\Delta n/V_{bed}$ (mol/m^3_{bed})	$qi(C_{in})$ (mol/m^3_{solid})
Co	3BV/h	6.94×10^{-8}	81.55	828.24	1996.15
Ni			308.04	6796.16	16,944.25
Co	6BV/h	9.26×10^{-8}	81.55	829.09	1998.32
Ni			308.042	5416.39	13,406.38
Co	9BV/h	4.63×10^{-8}	81.55	397.56	891.82
Ni			308.04	3426.96	8305.27

Table 5
Summary of breakthrough results for Co and Ni on Lewatit TP 220. Volumetric flow rate Q, the inlet concentration C_{in}, the total amount adsorbed in the column Δn, the corresponding amount per unit bed volume $\Delta n/V_{\text{bed}}$, and the equilibrium solid-phase concentration $q_i(C_{\text{in}})$.

Metal	Flow rate	Q (m^3/s)	$C_{in}\left(\frac{mol}{m^3}\right)$	$\Delta n/V_{bed}$ (mol/m^3_{bed})	$qi(C_{in})$ (mol/m^3_{solid})
Co	3BV/h	4.0×10^{-8}	8.4×10^1	2.0×10^2	3.9×10^2
Ni			8.4×10^1	8.1×10^2	2.0×10^3
Co	6BV/h	5.6×10^{-8}	8.4×10^1	2.3×10^2	4.5×10^2
Ni			8.4×10^1	5.7×10^2	1.3×10^3
Co	9BV/h	6.9×10^{-8}	8.4×10^1	2.7×10^2	5.7×10^2
Ni			8.4×10^1	5.0×10^2	1.2×10^3

calculates the depletion of renewable and non-renewable resources; and Mineral Resources Scarcity. For analysis, we considered the production of 1ton LiOH. Transportation of spent batteries, collection and storage are out of scope, as well as potential use of these materials for battery production. We understand that LCA requires more details and discussion as previously discussed in literature [14,20], but here our goal is to demonstrate a hydrometallurgical route design allied to environmental impact of the process proposed. We propose technical and environmental analysis for a new recycling process for Li-ion batteries. For the first time, such LCA includes the use of ozone for precipitation in a hydrometallurgical route, which is important for future implementations.

About 1.46×10^6 kg-CO_2eq would be generated to produce 1 ton of LiOH (Table S6) and energy consumption would primarily come from non-renewable fossil resources (18.8TJ, Table S7). Fossil CO_2 is the main air emission (91.8% of the emissions generated during the recycling route). N_2O represented 4.08% of emissions, followed by fossil methane (2.48%) and CO_2 (1.15%). Oxalic acid is responsible for 94.3% of the environmental impact generated by the developed route, which is in accordance with current organic acid production process that has higher environmental impact than inorganic acids [43]. Allied to experimental work, we proposed the separation and production of mixed hydroxide precipitate (Ni—Co) instead of oxalate compound (Fig. S4), and decision for the choice of oxalate or hydroxide will be made based on market. Regarding our data, the environmental impact is higher than previously reported in literature due to the complexity of steps and separation techniques [20,40,43], but it has potential to be lower than mining process with recovery of 95% of materials from spent batteries.

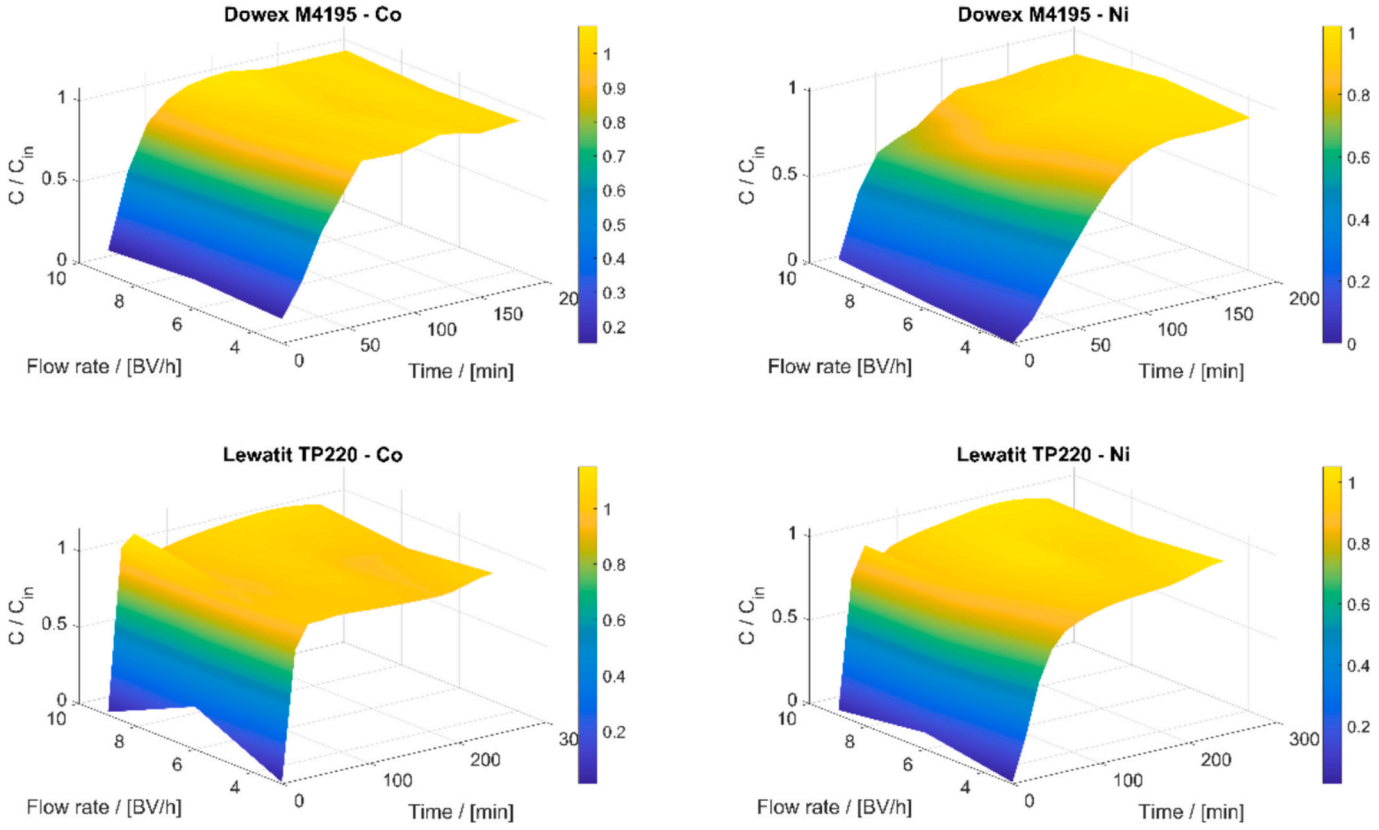

Fig. 5. 3D surface plots of Co and Ni breakthrough (C/C_{in}) as a function of time and flow rate for Dowex M4195 and Lewatit TP 220.

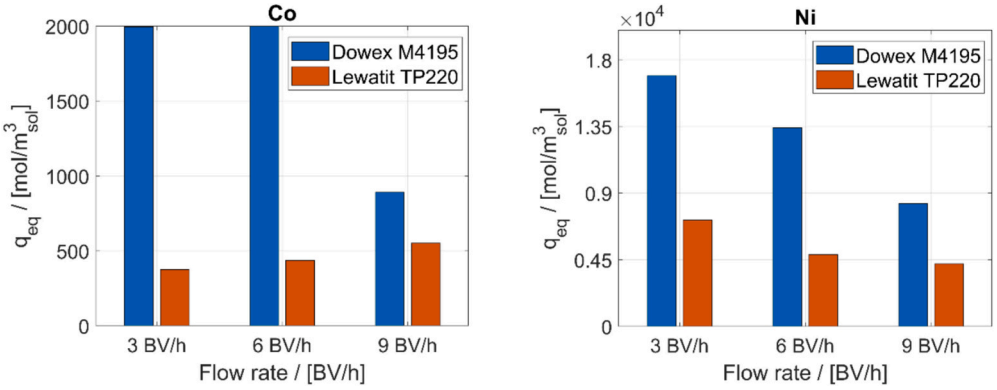

Fig. 6. Equilibrium capacities q_{eq} of Co and Ni on Dowex M4195 and Lewatit TP 220 resins at different flow rates.

For industrial scaling, a few challenges can be mentioned: ozone production from air (21% O_2) instead of concentrated oxygen gas (>90%) to reduce costs, and electricity consumption for ozone production; ion exchange chelating resin regeneration and the use of columns in series and in parallel; include in environmental assessment the impact of spent batteries generation and production of new batteries from the recycling process; and include new types for Ni-rich batteries (such as NMC 90.50.5 and LMO).

4. Conclusions

The aim of this paper was the development of a hydrometallurgical processing flowchart of NMC batteries with flexibility to recycle all types of Ni-rich batteries. Physical processing can be applied for different types of batteries (prismatic, pouch and cylindrical) to remove plastic, external structure, and foils (mostly Cu) fractions. In acid leaching of black mass, remained Al foil works as a better option for reducing agent than H_2O_2, where H_2SO_4 is still the best economic and environmental option. Mn precipitation by ozone reaches 99% efficiency with 96% purity (4% Co oxide) which represents a better option than solvent extraction considering losses of Co and extraction/stripping steps; however, time (5 h) and ozone consumption (3.0 L/min O_2) are challenges to be overcome in upscaling steps. Ion exchange chelating resins can be used for separation of Ni and Co over Al and Li. We demonstrated by experimental data and optimization modeling that differences in particle size of Dowex M4195 and Lewatit TP 220 impacts adsorption capacity even having the same functional group (bis-picolylamine). Oxalic precipitation represents a direct alternative for Ni and Co

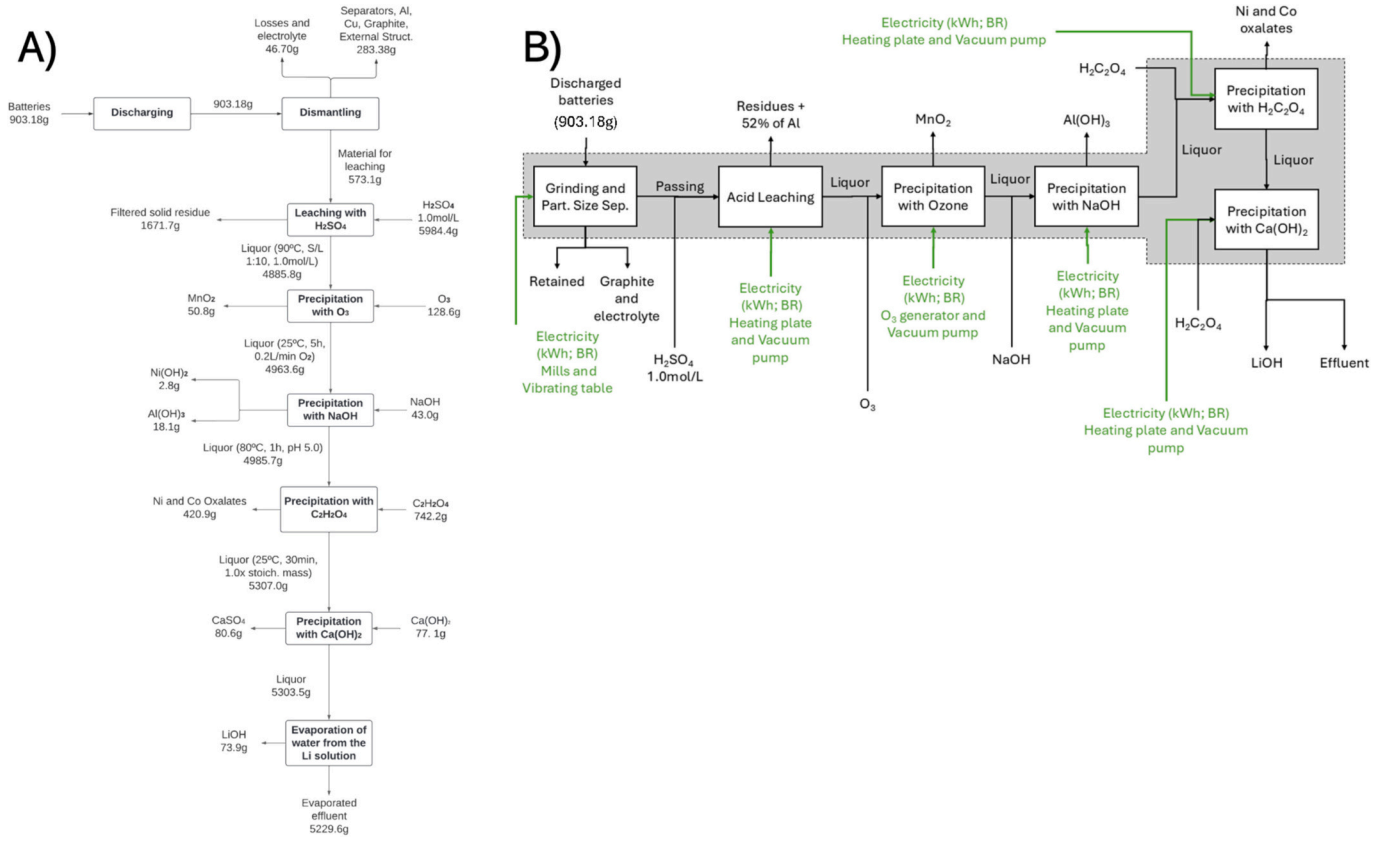

Fig. 7. a) Flowchart elaborated for recycling of NMC811-type cathode of Li-ion batteries by hydrometallurgical process; b) Process system considered for LCA. Mass balance considering almost 1 kg of Li-ion batteries used for the experiments in this work.

precipitation as mixed product after Al precipitation by NaOH, with slightly co-precipitation of Li (3.5%–5.1%). Sulfate ions were removed by precipitation to produce a high pure LiOH solution, but it can be easily replaced by electrochemical separation (e.g., electrodialysis). No detection of Na, Ca and Cl was observed in Ni—Co oxalate and LiOH. Recovery efficiencies were 99.2% for Mn, 94.6% for Ni, 96.3% for Co, and 87.8% for Li. Al recovery in hydrometallurgical processing was 99.1% considering recovery of foil particles after leaching. About 1.46 $\times$ 10^6 kg-CO_2eq would be generated to produce 1 ton of LiOH, lower than mining process with recovery of 95% battery materials.

CRediT authorship contribution statement

Lucas Fonseca Guimaraes: Validation, Methodology, Investigation, Formal analysis, Data curation. **Carine de Menezes Rebello:** Writing – original draft, Visualization, Validation, Software. **Idelfonso Bessa dos Reis Nogueira:** Writing – original draft, Visualization, Validation, Software. **Mentore Vaccari:** Supervision, Resources, Funding acquisition. **Denise Crocce Romano Espinosa:** Supervision, Project administration, Methodology, Investigation, Funding acquisition, Formal analysis. **Amilton Barbosa Botelho Junior:** Writing – review & editing, Writing – original draft, Visualization, Validation, Supervision, Project administration, Methodology, Investigation, Conceptualization.

Declaration of competing interest

The authors declare that they have no known competing financial interests or personal relationships that could have appeared to influence the work reported in this paper.

Acknowledgments

The authors thank the University of Sao Paulo for supporting this project and Fundação de Amparo à Pesquisa do Estado de São Paulo and Capes (2019/11866-5, 2021/ 14842-0, and 2023/01032-5) for the financial support. ABBJR would like to thank the Department of Chemical Engineering at NTNU for the financial support. Dilshan Premathilake and Teklit Ambaye for the support in LCA software and data discussion.

Appendix A. Supplementary data

Supplementary data to this article can be found online at https://doi.org/10.1016/j.cej.2026.173667.

Data availability

Data will be made available on request.

References

[1] S. Giljum, V. Maus, L. Sonter, S. Luckeneder, T. Werner, S. Lutter, J. Gershenzon, M.J. Cole, J. Siqueira-Gay, A. Bebbington, Metal mining is a global driver of environmental change, Nat. Rev. Earth Environ. 6 (2025) 441–455, https://doi.org/10.1038/s43017-025-00683-w.
[2] International Energy Agency, World Energy Outlook 2025. https://www.iea.org/reports/world-energy-outlook-2025, 2025.
[3] Mc Kinsey and Company, McKinsey materials transition : on Risk supply chains, 2023.
[4] E.A. Olivetti, G. Ceder, G.G. Gaustad, X. Fu, Lithium-ion battery supply chain considerations : analysis of potential bottlenecks in critical metals, Joule 1 (2017) 229–243, https://doi.org/10.1016/j.joule.2017.08.019.

[5] X. Ma, Z. Meng, M.V. Bellonia, J. Spangenberger, G. Harper, E. Gratz, E. Olivetti, R. Arsenault, Y. Wang, The evolution of lithium-ion battery recycling, Nat. Rev. Clean Technol. 1 (2025) 75–94, https://doi.org/10.1038/s44359-024-00010-4.
[6] C. Xu, Q. Dai, L. Gaines, M. Hu, A. Tukker, B. Steubing, Future material demand for automotive lithium-based batteries, Commun. Mater. 1 (2020), https://doi.org/10.1038/s43246-020-00095-x.
[7] S.H. Ali, The US should get serious about mining critical minerals for clean energy, Nature 615 (2023) 563, https://doi.org/10.1038/d41586-023-00790-y.
[8] S.H. Ali, D. Giurco, N. Arndt, E. Nickless, G. Brown, A. Demetriades, R. Durrheim, M.A. Enriquez, J. Kinnaird, A. Littleboy, L.D. Meinert, R. Oberhänsli, J. Salem, R. Schodde, G. Schneider, O. Vidal, N. Yakovleva, Mineral supply for sustainable development requires resource governance, Nature 543 (2017) 367–372, https://doi.org/10.1038/nature21359.
[9] D. Raabe, C.C. Tasan, E.A. Olivetti, Strategies for improving the sustainability of structural metals, Nature 575 (2019) 64–74, https://doi.org/10.1038/s41586-019-1702-5.
[10] Mine and monitor impacts, Nat. Geosci. 8 (2015) 161, https://doi.org/10.1038/ngeo2390.
[11] D. Fuentealba, C. Flores-Fernández, E. Troncoso, H. Estay, Technological tendencies for lithium production from salt lake brines: Progress and research gaps to move towards more sustainable processes, Res. Policy 83 (2023) 103572, https://doi.org/10.1016/j.resourpol.2023.103572.
[12] M.L. Vera, W.R. Torres, C.I. Galli, A. Chagnes, V. Flexer, Environmental impact of direct lithium extraction from brines, Nat. Rev. Earth Environ. 4 (2023) 149–165, https://doi.org/10.1038/s43017-022-00387-5.
[13] A.B. Botelho Junior, F.P. Martins, L.O. Cezarino, L.B. Liboni, J.A.S. Tenório, D.C. R. Espinosa, The sustainable development goals, urban mining, and the circular economy, Extr. Ind. Soc. 16 (2023) 101367, https://doi.org/10.1016/j.exis.2023.101367.
[14] M.L. Machala, X. Chen, S.P. Bunke, G. Forbes, A. Yegizbay, J.A. de Chalendar, I. L. Azevedo, S. Benson, W.A. Tarpeh, Life cycle comparison of industrial-scale lithium-ion battery recycling and mining supply chains, Nat. Commun. 16 (2025) 988, https://doi.org/10.1038/s41467-025-56063-x.
[15] L.F. Guimarães, J.A.S. Tenório, M. Vaccari, D.C.R. Espinosa, A.B. Botelho Junior, Characterization of Lithium-ion batteries from recycling perspective towards circular economy, Minerals 14 (2024) 1–22, https://doi.org/10.3390/min14090878.
[16] A.B. Botelho Junior, Sustainable mining – unlocking resources towards circular economy to meet energy transition through electrochemistry, J. Environ. Chem. Eng. 13 (2025) 116600, https://doi.org/10.1016/j.jece.2025.116600.
[17] L.S. Martins, L.F. Guimarães, A.B. Botelho Junior, J.A.S. Tenório, D.C.R. Espinosa, Electric car battery: an overview on global demand, recycling and future approaches towards sustainability, J. Environ. Manag. 295 (2021) 113091, https://doi.org/10.1016/j.jenvman.2021.113091.
[18] J. Lim, Y. Jang, J. Lee, C. Lee, O. Jbari, K. Kwon, E. Chung, Hydrometallurgical process of spent lithium-ion battery recycling part. 2 recovery of valuable metals from the cathode active material leachates: review and cost analysis, Hydrometallurgy 236 (2025) 106516, https://doi.org/10.1016/j.hydromet.2025.106516.
[19] Y. Ning, Y. Zhang, H. Li, Z. Yu, G. Wei, J. Qu, Recovery of valuable metals from LiNixCoyMnzO2 and LiFePO4 mixed leachate based on thermodynamic calculations and experimental optimization, J. Water Process Eng. 71 (2025) 107274, https://doi.org/10.1016/j.jwpe.2025.107274.
[20] F. Duarte Castro, E. Mehner, L. Cutaia, M. Vaccari, Life cycle assessment of an innovative lithium-ion battery recycling route: a feasibility study, J. Clean. Prod. 368 (2022) 133130, https://doi.org/10.1016/j.jclepro.2022.133130.
[21] L. Schlott, M. Gutsch, J. Leker, Cost modelling and key drivers in lithium-ion battery recycling, Nat. Rev. Clean Technol. (2025), https://doi.org/10.1038/s44359-025-00095-5.
[22] G. Zhu, Q. Yang, X. Guo, D. Yu, A.M. Mitrašinović, Q. Tian, H. Feng, K. Zhang, Selective lithium recovery from spent NCM type Li-ion battery materials by powder electrolysis, J. Environ. Chem. Eng. 13 (2025) 1–11, https://doi.org/10.1016/j.jece.2024.115173.
[23] X. Wei, Z. Guo, Y. Zhao, Y. Sun, A. Hankin, M. Titirici, Recovery of graphite from industrial lithium-ion battery black mass, RSC Sustain. 3 (2024) 264–274, https://doi.org/10.1039/d4su00427b.
[24] M.E. de M.G. Dias, J.A.S. Tenório, D.C.R. Espinosa, A.B. Botelho Junior, Recycling of Li-ion batteries: recovery of critical metals by hydrometallurgy, JOM 111 (2025), https://doi.org/10.1007/s11837-025-07677-5, 0–11.
[25] L.F. Guimarães, A.B. Botelho Junior, D.C.R. Espinosa, Sulfuric acid leaching of metals from waste Li-ion batteries without using reducing agent, Miner. Eng. 183 (2022) 107597, https://doi.org/10.1016/j.mineng.2022.107597.
[26] R.H. de Castro, D.C.R. Espinosa, L.A. Gobo, E.A. Kumoto, A.B. Botelho Junior, J.A. S. Tenorio, Design of Recycling Processes for NCA-type Li-ion batteries from electric vehicles toward the circular economy, Energy Fuel 38 (2024) 5545–5557, https://doi.org/10.1021/acs.energyfuels.3c04904.
[27] W. Chu, Y.L. Zhang, X. Chen, Y.G. Huang, H.Y. Cui, M. Wang, J. Wang, Synthesis of LiNi0.6Co0.2Mn0.2O2 from mixed cathode materials of spent lithium-ion batteries, J. Power Sources 449 (2020) 227567, https://doi.org/10.1016/j.jpowsour.2019.227567.
[28] G. Harper, R. Sommerville, E. Kendrick, L. Driscoll, P. Slater, R. Stolkin, A. Walton, P. Christensen, O. Heidrich, S. Lambert, A. Abbott, K. Ryder, L. Gaines, P. Anderson, Recycling lithium-ion batteries from electric vehicles, Nature 575 (2019) 75–86, https://doi.org/10.1038/s41586-019-1682-5.
[29] D.R. Guillén, J. Guimarães Sanches, A.B. Botelho Junior, L.A. Gobo, M. G. Bergerman, D.C.R. Espinosa, J.A.S. Tenório, Physical process for Li-ion battery recycling from electric vehicles, Ind. Eng. Chem. Res. 63 (2024) 19788–19803, https://doi.org/10.1021/acs.iecr.4c03271.
[30] J. Mao, C. Ye, S. Zhang, F. Xie, R. Zeng, K. Davey, Z. Guo, S. Qiao, Toward practical lithium-ion battery recycling: adding value, tackling circularity and recycling-oriented design, Energy Environ. Sci. 15 (2022) 2732–2752, https://doi.org/10.1039/d2ee00162d.
[31] X. Yu, W. Li, V. Gupta, H. Gao, D. Tran, S. Sarwar, Z. Chen, Current challenges in efficient Lithium-ion batteries' recycling: a perspective, Global Chall. 6 (2022), https://doi.org/10.1002/gch2.202200099.
[32] A. Locati, M. Mikulić, L.M.J. Rouquette, B. Ebin, M. Petranikova, Production of high purity MnSO4·H2O from real NMC111 Lithium-ion batteries leachate using solvent extraction and evaporative crystallization, Solvent Extr. Ion Exch. 42 (2024) 636–657, https://doi.org/10.1080/07366299.2024.2435272.
[33] N. Vieceli, C. Vonderstein, T. Swiontekc, S. Stopić, C. Dertmann, R. Sojka, N. Reinhardt, C. Ekberg, B. Friedrich, M. Petranikova, Recycling of Li-ion batteries from industrial processing: Upscaled hydrometallurgical treatment and recovery of high purity manganese by solvent extraction, Solvent Extraction and Ion Exchange 41 (2023) 205–220, https://doi.org/10.1080/07366299.2023.2165405.
[34] J.M. de A. Sales, A.B. Botelho Junior, L.A. Gobo, E.A. Kumoto, D.C.R. Espinosa, J.A. S. Tenório, Precipitation of manganese by ozone from hydrometallurgical recycling process of lithium-ion batteries, J. Clean. Prod. 434 (2024) 140099, https://doi.org/10.1016/j.jclepro.2023.140099.
[35] G.M. Mudd, Sustainable/responsible mining and ethical issues related to the sustainable development goals, Geol. Soc. Spec. Publ. 508 (2021) 187–199, https://doi.org/10.1144/SP508-2020-113.
[36] N.B.R. Monteiro, E.A. da Silva, J.M. Moita Neto, Sustainable development goals in mining, J. Clean. Prod. 228 (2019) 509–520, https://doi.org/10.1016/j.jclepro.2019.04.332.
[37] J. Vänskä, J. Partinen, Y. Zou, M. Lundström, Leaching of lithium iron phosphate in the presence of cu and Al in mild sulfuric acid solutions, J. Sustain. Metall. (2025), https://doi.org/10.1007/s40831-025-01159-3.
[38] J. Partinen, P. Halli, A. Varonen, B.P. Wilson, M. Lundström, Investigating battery black mass leaching performance as a function of process parameters by combining leaching experiments and regression modeling, Miner. Eng. 215 (2024), https://doi.org/10.1016/j.mineng.2024.108828.
[39] M. Roshanfar, M. Sartaj, S. Kazemeini, A greener method to recover critical metals from spent lithium-ion batteries (LIBs): synergistic leaching without reducing agents, J. Environ. Manag. 366 (2024) 121862, https://doi.org/10.1016/j.jenvman.2024.121862.
[40] R. Golmohammadzadeh, F. Rashchi, E. Vahidi, Recovery of lithium and cobalt from spent lithium-ion batteries using organic acids: process optimization and kinetic aspects, Waste Manag. 64 (2017) 244–254, https://doi.org/10.1016/j.wasman.2017.03.037.
[41] G.P. Nayaka, K.V. Pai, G. Santhosh, J. Manjanna, Recovery of cobalt as cobalt oxalate from spent lithium ion batteries by using glycine as leaching agent, J. Environ. Chem. Eng. 4 (2016) 2378–2383, https://doi.org/10.1016/j.jece.2016.04.016.
[42] L.S. Martins, S. Rovani, A.B. Botelho Junior, D.C. Romano Espinosa, Sustainable approach for critical metals recovery through hydrometallurgical processing of spent batteries using organic acids, Ind. Eng. Chem. Res. 62 (2023) 18672–18682, https://doi.org/10.1021/acs.iecr.3c03048.
[43] S. Mousavinezhad, S. Kadivar, E. Vahidi, Comparative life cycle analysis of critical materials recovery from spent Li-ion batteries, J. Environ. Manag. 339 (2023) 117887, https://doi.org/10.1016/j.jenvman.2023.117887.
[44] M. Rinne, R. Aromaa-Stubb, H. Elomaa, A. Porvali, M. Lundström, Evaluation of hydrometallurgical black mass recycling with simulation-based life cycle assessment, Int. J. Life Cycle Assess. (2024), https://doi.org/10.1007/s11367-024-02304-y.
[45] T. Wesselborg, S. Asumalahti, S. Virolainen, T. Sainio, Design of a continuous ion exchange process in battery metals recycling: from single column experiments towards a simulated moving bed configuration, Hydrometallurgy 228 (2024) 106361, https://doi.org/10.1016/j.hydromet.2024.106361.
[46] D.C.R. Espinosa, J.A.S. Tenório, A.B. Botelho Junior, A.M.N. de O. Lima, D. da S. Vasconcelos, J.M. de A. Sales, S. Rovani, M.E. de M.G. Dias, R.H. de Castro, L. A. Gobo, E.A. Kumoto, Battery recycling process, PCT/BR2023/050069, 2023.
[47] B.P. Oruê, A.B. Botelho Junior, J.A.S. Tenório, D.C.R. Espinosa, M. dos P.G. Baltazar, Kinetic study of manganese precipitation of nickel laterite leach based-solution by ozone oxidation, Ozone Sci. Eng. 43 (2021) 324–338, https://doi.org/10.1080/01919512.2020.1796580.
[48] P. Meshram, S. Virolainen, A. Abhilash, T. Sainio, Solvent extraction for separation of 99.9% pure cobalt and recovery of Li, Ni, Fe, cu, Al from spent LIBs, Metals (Basel). 12 (2022) 1056, https://doi.org/10.3390/met12061056.
[49] D.P. Mantuano, G. Dorella, R.C.A. Elias, M.B. Mansur, Analysis of a hydrometallurgical route to recover base metals from spent rechargeable batteries by liquid-liquid extraction with Cyanex 272, J. Power Sources 159 (2006) 1510–1518, https://doi.org/10.1016/j.jpowsour.2005.12.056.
[50] A. Verma, A.J. Henne, D.R. Corbin, M.B. Shiflett, Lithium and cobalt recovery from LiCoO 2 using oxalate chemistry: scale-up and techno-economic analysis, Ind. Eng. Chem. Res. 61 (2022) 5285–5294, https://doi.org/10.1021/acs.iecr.1c04876.
[51] M.H. Ibrahim, D. Batstone, J. Vaughan, K. Steel, Electrochemical separation of sulfuric acid from magnesium sulfate solutions: application for nickel laterite processing, Sep. Purif. Technol. 336 (2024) 126291, https://doi.org/10.1016/j.seppur.2024.126291.
[52] M.H. Ibrahim, D.J. Batstone, J. Vaughan, K. Steel, Understanding sulfate transport phenomena during electrochemical acid recovery from waste MgSO4: a modelling

approach, Sep. Purif. Technol. 360 (2025) 130988, https://doi.org/10.1016/j.seppur.2024.130988.
[53] I.B.R. Nogueira, R.P.V. Faria, R. Requião, H. Koivisto, M.A.F. Martins, A. E. Rodrigues, J.M. Loureiro, A.M. Ribeiro, Chromatographic studies of n-propyl propionate: adsorption equilibrium, modelling and uncertainties determination, Comput. Chem. Eng. 119 (2018) 371–382, https://doi.org/10.1016/j.compchemeng.2018.09.020.
[54] D.S. Premathilake, T.G. Ambaye, A.B. Botelho Junior, A.T.M. Lima, D.C. R. Espinosa, M. Vaccari, Comparative environmental and economic assessment of emerging hydrometallurgical recycling technologies for Li-ion battery cathodes, Sustainable Prod. Consumption 51 (2024) 327–344, https://doi.org/10.1016/j.spc.2024.09.015.
[55] T. Watari, K. Nansai, K. Nakajima, Major metals demand, supply, and environmental impacts to 2100: a critical review, Resour. Conserv. Recycl. 164 (2021) 105107, https://doi.org/10.1016/j.resconrec.2020.105107.
[56] L. Peiseler, V. Schenker, K. Schatzmann, S. Pfister, V. Wood, T. Schmidt, Carbon footprint distributions of lithium-ion batteries and their materials, Nat. Commun. 15 (2024) 10301, https://doi.org/10.1038/s41467-024-54634-y.
[57] E.C. Giese, Strategic minerals: global challenges post-COVID-19, Extr. Ind. Soc. (2022) 101113, https://doi.org/10.1016/j.exis.2022.101113.
[58] R. Chenitz, E. Pajootan, A. Mokrini, Future of battery grade graphite recycling from spent batteries, ACS Sustain. Resour. Manag. (2025) 5–7, https://doi.org/10.1021/acssusresmgt.5c00312.
[59] N. Vieceli, T. Ottink, S. Stopic, C. Dertmann, T. Swiontek, C. Vonderstein, R. Sojka, N. Reinhardt, C. Ekberg, B. Friedrich, M. Petranikova, Solvent extraction of cobalt from spent lithium-ion batteries: dynamic optimization of the number of extraction stages using factorial design of experiments and response surface methodology, Sep. Purif. Technol. 307 (2023), https://doi.org/10.1016/j.seppur.2022.122793.
[60] Z.T. Ichlas, M.Z. Mubarok, A. Magnalita, J. Vaughan, A.T. Sugiarto, Processing mixed nickel-cobalt hydroxide precipitate by sulfuric acid leaching followed by selective oxidative precipitation of cobalt and manganese, Hydrometallurgy 191 (2020) 105185, https://doi.org/10.1016/j.hydromet.2019.105185.
[61] I.R. Rodrigues, C. Deferm, K. Binnemans, S. Riaño, Separation of cobalt and nickel via solvent extraction with Cyanex-272: batch experiments and comparison of mixer-settlers and an agitated column as contactors for continuous counter-current extraction, Sep. Purif. Technol. 296 (2022) 121326, https://doi.org/10.1016/j.seppur.2022.121326.
[62] CYTEC, CYANEX 272 Extractant, (2008) 16. http://www.cytec.com/sites/default/files/datasheets/CYANEX 272 Brochure.pdf (accessed January 16, 2018).
[63] Z.T. Ichlas, D.C. Ibana, Process development for the direct solvent extraction of nickel and cobalt from nitrate solution: aluminum, cobalt, and nickel separation using Cyanex 272, Int. J. Miner. Metall. Mater. 24 (2017) 37–46, https://doi.org/10.1007/s12613-017-1376-7.
[64] P.E. Tsakiridis, S. Agatzini-Leonardou, Solvent extraction of aluminium in the presence of cobalt, nickel and magnesium from sulphate solutions by Cyanex 272, Hydrometallurgy 80 (2005) 90–97, https://doi.org/10.1016/j.hydromet.2005.07.002.
[65] A.S. Guimarães, M.B. Mansur, Removal of Mg and ca from Ni-rich sulphate solutions by solvent extraction using cationic and neutral extractants, Miner. Eng. 185 (2022) 1–11, https://doi.org/10.1016/j.mineng.2022.107684.
[66] A.S. Guimarães, M.B. Mansur, Selection of a synergistic solvent extraction system to remove calcium and magnesium from concentrated nickel sulfate solutions, Hydrometallurgy 175 (2018) 250–256, https://doi.org/10.1016/j.hydromet.2017.12.001.
[67] S. Virolainen, T. Wesselborg, A. Kaukinen, T. Sainio, Removal of iron, aluminium, manganese and copper from leach solutions of lithium-ion battery waste using ion exchange, Hydrometallurgy 202 (2021) 105602, https://doi.org/10.1016/j.hydromet.2021.105602.
[68] S. Gmar, L. Muhr, F. Lutin, A. Chagnes, Lithium-ion battery recycling: metal recovery from electrolyte and cathode materials by electrodialysis, Metals (Basel) 12 (2022), https://doi.org/10.3390/met12111859.
[69] M.L. Strauss, L.A. Diaz, J. McNally, J. Klaehn, T.E. Lister, Separation of cobalt, nickel, and manganese in leach solutions of waste lithium-ion batteries using Dowex M4195 ion exchange resin, Hydrometallurgy 206 (2021) 105757, https://doi.org/10.1016/j.hydromet.2021.105757.
[70] M. Streat, APPLICATIONS OF ION EXCHANGE IN HYDROMETALLURGY, 1986, pp. 449–461.
[71] M.L. Inamuddin, Ion Exchange Technology I, Springer Netherlands, Dordrecht, 2012, https://doi.org/10.1007/978-94-007-1700-8.
[72] M.V. Dinu, E.D. Comăniţă, E.S. Drăgan, Kinetic study on heavy metals adsorption by iminodiacetate chelating resins, Environ. Eng. Manag. J. 11 (2012) 1587–1594.
[73] S. Edebali, E. Pehlivan, Evaluation of chelate and cation exchange resins to remove copper ions, Powder Technol. 301 (2016) 520–525, https://doi.org/10.1016/j.powtec.2016.06.011.
[74] E.A. Ajiboye, V. Aishvarya, J. Petersen, Selective recovery of copper from the mixed metals leach liquor of E-waste materials by ion-exchange: batch and column study, Minerals 13 (2023) 1285, https://doi.org/10.3390/min13101285.
[75] A. Bringas, E. Bringas, R. Ibañez, Ma.-F. San-Román, Fixed-bed columns mathematical modeling for selective nickel and copper recovery from industrial spent acids by chelating resins, Sep. Purif. Technol. 313 (2023) 123457, https://doi.org/10.1016/j.seppur.2023.123457.
[76] F.K. Crundwell, M.S. Moats, V. Ramachandran, T.G. Robinson, W.G. Davenport, Extractive Metallurgy of Nickel, Cobalt and Platinum-Group Metals, First, Elsevier, Oxford, 2011.
[77] H. Kay, Treatment of Nickelliferous Oxidic Materials for the Recovery of Nickel Values, 3,466,144, 1969.
[78] N.C. Zeballos, W.R. Torres, C.H. Díaz Nieto, V. Flexer, In situ production of carbonate anions from water electrolysis and CO2 absorption for Li2CO3 crystallization from preconcentrated brines, Ind. Eng. Chem. Res. (2024), https://doi.org/10.1021/acs.iecr.4c02193.
[79] X. Zeng, J. Li, B. Shen, Novel approach to recover cobalt and lithium from spent lithium-ion battery using oxalic acid, J. Hazard. Mater. 295 (2015) 112–118, https://doi.org/10.1016/j.jhazmat.2015.02.064.
[80] A.F. Mayta-armas, D. Crocce, R. Espinosa, J. Alberto, S. Ten, Li separation by electrodialysis in hydrometallurgical processing of Li-ion batteries : a review of the state-of-art, Miner. Eng. 234 (2025) 1–16, https://doi.org/10.1016/j.mineng.2025.109720.
[81] A.F. Mayta-Armas, D.C.R. Espinosa, J.A.S. Tenório, A.B. Botelho Junior, Membrane-based electrochemical separation: effect of co-ions on Li separation in battery recycling, Sep. Purif. Technol. 382 (2026) 135766, https://doi.org/10.1016/j.seppur.2025.135766.
[82] M.M. Jiménez Correa, Separação de cobre, níquel e cobalto de um licor produzido na lixiviação de minério laterítico de níquel usando resinas quelantes, Universidade de São Paulo (2020), https://doi.org/10.11606/T.3.2020.tde-08012020-162904.
[83] A.B. Botelho Junior, D.C.R. Espinosa, D. Dreisinger, J.A.S. Tenório, Recovery of nickel and cobalt from nickel laterite leach solution using chelating resins and pre-reducing process, Can. J. Chem. Eng. 97 (2019) 1181–1190, https://doi.org/10.1002/cjce.23359.
[84] A.B. Botelho Junior, A. de A. Vicente, D.C.R. Espinosa, J.A.S. Tenório, Recovery of metals by ion exchange process using chelating resin and sodium dithionite, J. Mater. Res. Technol. 8 (2019) 4464–4469, https://doi.org/10.1016/j.jmrt.2019.07.059.
[85] A.B. Botelho Junior, D.B. Dreisinger, D.C.R. Espinosa, J.A.S. Tenório, Pre-reducing process kinetics to recover metals from nickel leach waste using chelating resins, Int. J. Chem. Eng. 2018 (2018) 1–7, https://doi.org/10.1155/2018/9161323.
[86] H. Ji, J. Wang, J. Ma, H.M. Cheng, G. Zhou, Fundamentals, status and challenges of direct recycling technologies for lithium ion batteries, Chem. Soc. Rev. 52 (2023) 8194–8244, https://doi.org/10.1039/d3cs00254c.
[87] D. da S. Vasconcelos, D.C. Romano Espinosa, J.A.S. Tenório, A.B. Botelho Junior, L. A. Gobo, Hydrometallurgical strategy to reduce waste through the recycling of lithium iron phosphate batteries, ACS Omega (2025), https://doi.org/10.1021/acsomega.5c07786.